Dynamic modeling of a liquid piston compressor system including conjugate heat transfer

Mathieu Specklin[1] Elie Solai[2] Clémence Rouge[3] Michael Deligant[2]

[1]Cnam, Arts et Metiers Institute of Technology, LIFSE, Paris, F-75013, France
[2]Arts et Metiers Institute of Technology, Cnam, LIFSE, Paris, F-75013, France
[3]Université Bourgogne Europe, DRIVE UR 1859, 58000 Nevers, France

Abstract

Efficient and cost-effective hydrogen storage necessitates quick compression across significant pressure ranges (usually up to 700 bar), while keeping heat generation to a minimum during the process. This can be achieved by improved understanding of gas-to-wall heat transfer enhancement in hydrogen compression systems, careful design and operational optimisation. In this context, the present paper introduces a 0D/1D lumped numerical model of a liquid piston compressor for hydrogen applications. Heat transfer is considered as (i) convective at the liquid-gas interface, (ii) conductive within the gas volume based on a 1D approach accounting for thermal stratification, and (iii) as conjugate at the gas-to-wall interface. To achieve a pressure ratio of 30 (from 15 to 450) bar, at a power density of approximately $65kW/m^3$, the compression energy cost reaches $1.85kWh/kg$. Further, various standard pressure vessels materials with different thermal and mechanical properties are considered, highlighting the potential compromise between lightweight and thermal efficiency.

Keywords:liquid-piston compressor, hydrogen, conjugate heat transfer

1 Introduction

Hydrogen holds great promise as an energy carrier that can progressively transition energy systems from relying on limited fossil fuels to utilizing sustainable renewable sources. It seeks to replace natural gas for domestic space heating and hot water, and enable long-range clean transportation. A major hurdle is achieving high-density hydrogen storage, particularly for hydrogen-powered vehicles that need to compete with the quick refueling and extensive range of traditional liquid fuel engines. A significant technical and economic obstacle for the transportation sector is the need to develop affordable compression, storage, and dispensing (CSD) stations outfitted with high-pressure compressors. Ideally, the hydrogen compression process should be isothermal, both to reduce the input work required and maintain the hydrogen delivery temperature very low (close to -40^oC). With limited heat transfer from the gas, this however comes at the expense of power density. Piston compressors are typically used in CSD stations as they are able to achieve high pressure ratios. In order to optimise simultaneously the piston compressors efficiency and power density, a compromise must be found.

Various methods have been developed to achieve near-isothermal compression in piston systems. Saadat et al. have concentrated on optimizing compression and expansion processes and maximizing heat transfer (Saadat, P. Li, and Simon 2012). Spraying liquid droplets can also enhance heat transfer by increasing the surface area between the gas and a secondary cooling fluid (Sapin et al. 2018). However, the energy required for injecting liquid droplets rises significantly with pressure. Another approach involves using phase change materials (PCMs) in the reservoir walls, where the heat from gas compression is stored isothermally as latent heat (Mazzucco et al. 2016). Recent focus has been on liquid-piston compressors, which replace the traditional reciprocating solid piston with a column of liquid, typically water, driven by a hydraulic pump. These systems offer excellent sealing and compatibility with heat transfer enhancers (Van de Ven and P. Y. Li 2009). An example of such enhancers is porous metal foams with high thermal inertia, which increase the heat transfer surface area when placed in the tank (Wieberdink et al. 2018). Finally, Specklin et al. investigated the potential of heat transfer augmentation with forced internal convection (Specklin et al. 2022).

In this paper, a comprehensive dynamic model is derived and used to investigate the role of the conjugate gas-to-wall heat transfer in the final energy cost of high pressure hydrogen compression. The model is based on the combination of 0D zonal approaches and a 1D discretization technique of the gas volume using elements from the Modelica Standard Library (MSL) (*MSL* 2023), in order to account for the different energy balances. The effect of different materials' thermal properties onto the heat transfer efficiency is put in parallel with their mechanical properties, especially the density, in order to give insight on potential optimal configurations. The study is introduced by presenting the composition and operation of a dual system of liquid piston compressors. Then, the main sub-models with their inherent governing equations are detailled. Finally, the thermodynamical behaviour of the system is hilighted and the final energy costs are assessed for different wall materials.

2 Modeling methodology

The current numerical model is constructed following the same principle as the full scale setup described in (Solai, Specklin, and Deligant 2025), originally working with air. A simple zonal 0D approach was proposed and used to assess the system compression efficiency through uncertainty analysis. This approach is extended here, the main improvements being:

- mimicking the dynamic behavior of the full test bench which includes a dual system of liquid piston,
- adapted for hydrogen gas,
- proposing a 1D discretization of the time-varying hydrogen gas volume accounting for temperature gradients,
- based on an innovative extension of the thermal components of MSL.

This modeling strategy is implemented and tested with OpenModelica (*OpenModelica* 2023).

2.1 Liquid piston compressor system

The present liquid piston compressor is designed with a dual system of pistons, which facilitates the compression-expansion operation. The full system is represented in a schematic diagram in Figure 1. The liquid piston compressor is operated via the control of four solenoid valves. The opening of the valves is cyclic and the switch is determined based on the water level. The solenoid valves operate in parallel by pairs, as water from one tank is pumped into the other one. The check valves at the top of the reservoirs allow to bound the internal pressure between the two extrema given by the boundary conditions. Hence, as the water level increases in one of the cylindrical tank, the gas is being compressed. Once the final (or maximum) pressure is reached during compression, the corresponding check valve opens and the compressed gas is discharged. During the expansion process, the water level decreases and consequently the pressure too. Similarly, if the initial (or minimum) pressure is reached, the opening of the check valve occurs and the tank is filled with gas at this minimum pressure.

The liquid-piston system model shown in Figure 1 is constructed from components from MSL and from the in-house developed library based on MSL components (*MSL* 2023). Check valves, solenoid valves and the volumetric pump are considered as ideal. The thermodynamic behaviour of both left and right liquid piston cylinders are described in the next section.

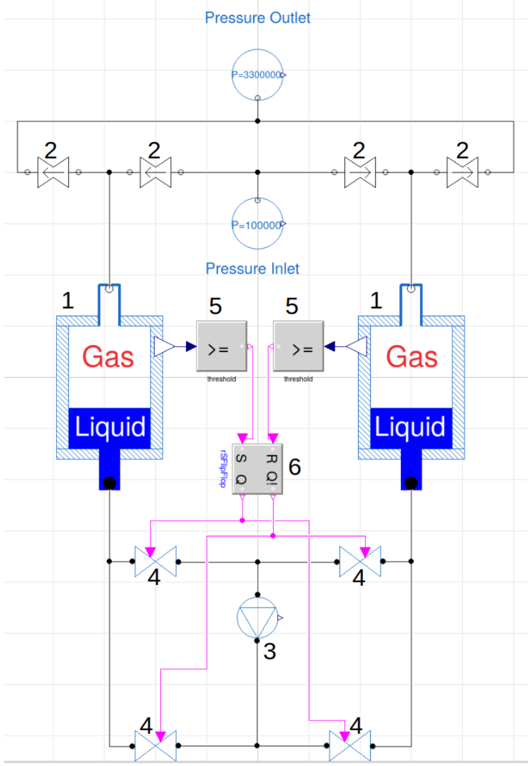

Figure 1. Schematic view of the experimental setup. 1) liquid piston tanks. 2) check valves. 3) volumetric pump. 4) solenoid control valves. 5) level threshold. 6) logical Reset-Set flipflop.

2.2 Components modeling and governing equations

The liquid piston gas-spring arrangement, described in Figure 2, is initially filled with hydrogen at $P_0 = 15$ bar and at $T_0 = 20$ °C. Water is injected to compress the gas contained within the cylinder up to a pressure of 450 bar, which corresponds to a pressure ratio of 30. During compression, the hydrogen is heated up by the boundary work applied by the liquid piston motion, while being cooled down by the gas-to-solid and gas-to-liquid heat transfers. Further, heat transfer by conduction within the hydrogen gas is considered in the vertical direction.

The liquid piston cylinder model is composed of two sub-models, one for both time-varying gas and liquid volumes, as illustrated in Figure 3. Conjugate heat transfer is considered with two half thermal resistor and a heat capacitor representing the thermal inertia of the wall.

The outer half resistance includes both conductive thermal resistance through half thickness of the solid wall and the convective thermal resistance with the ambient. The inner half resistance includes the same conductive resistance and convective thermal resistances with the gas volume and the liquid volumes. The conductive resistances consist of resistances due to the lateral cylinder surface (Patil, Acharya, and Ro 2019). The convective thermal resistance with the ambient is governed by a heat transfer coefficient fixed to a standard value of $5W.K^{-1}.m^{-2}$ for natural convection. Finally, the inner convective resistances associated to both fluids are time-dependent and their inherent heat transfer coefficients are computed based on Reynolds-Prandtl correlations:

DOI
10.3384/ecp2181001

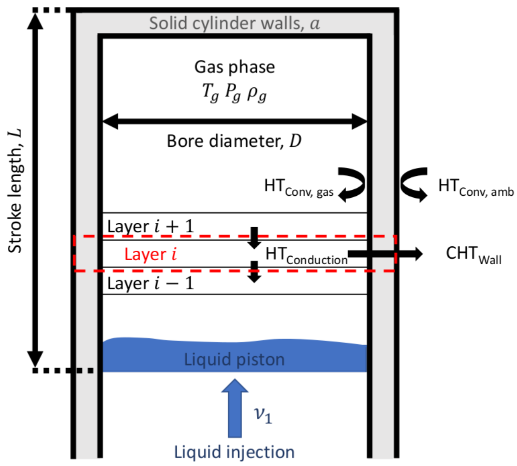

Figure 2. Schematic view of the liquid-piston cylinder involving 1D discretization of the gas volume.

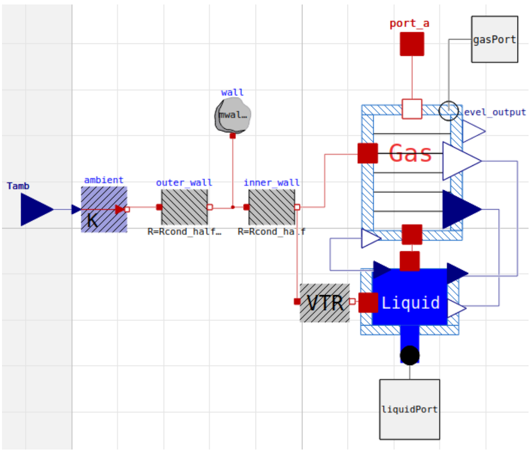

Figure 3. Schematic diagram of the liquid-piston cylinder model and its sub-models. The following variables are transfered between the sub-models of the gas and liquid volumes: the gas pressure P_g, the liquid volume V_l and the gas-to-liquid heat transfer coefficient h_{gl}.

$$Nu = aRe^bPr^c \tag{1}$$

where Nu is the Nusselt number. More specifically, for the liquid-to-wall heat transfer, a, b and c coefficients are fixed considering standard correlation for forced convection in laminar regime over a flat plate. As for the gas-to-wall heat transfer the coefficient values are adjusted based on the uncertainty quantification approach described in (Solai, Specklin, and Deligant 2025) for the same piston liquid system operating at similar conditions, yet with air. Both Reynolds Re and Prandtl Pr numbers are computed based on the instantaneous values of the thermophysical gas properties, which are all obtained with the hydrogen ideal gas media from MSL.

The volume of the gas is further decomposed by an array of layers that encompass the internal convective heat transfer described above. This 1D approach allows to account for the thermal gradient in the vertical dimension.

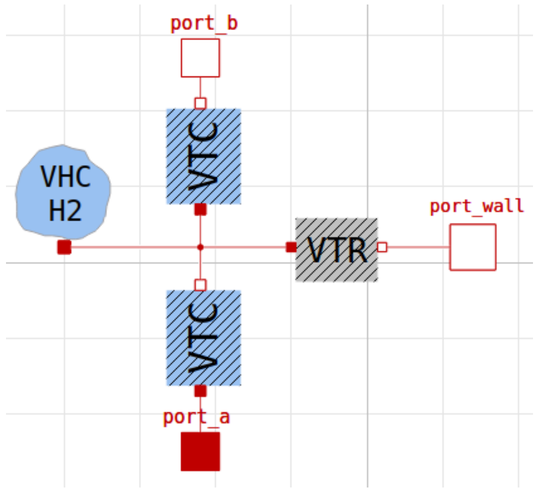

Figure 4. Schematic diagram of the gas layer element which includes convective thermal resistance with the adjacent wall. VHC stands for Variable Heat Capacitor, VTC stands for Variable Thermal Conductor and VTR stands for Variable Thermal Resistor.

A gas layer is thus made of the following element: a heat capacitor for the mass of hydrogen, two thermal conductors for conduction with the bottom and top gas layers, and the thermal resistor accounting for gas-to-wall heat transfer. The layer composition is shown in Figure 4. This is a modeling approach typically used for wall elements (Şeren and İpek 2023). In order to obtain a 1D discretization of the gas volume, these elements are defined as an array and connected successively. Another possibility lies in the direct resolution of the 1D partial differential equation such as in (Maccarini et al. 2023). In the present paper, the gas layer elements account for the time variation of the gas volume and thermodynamical properties during compression, expansion, discharge and admission stages. Hence, the different thermal components are extended versions of the MSL equivalent components with time-varying inputs governing their thermodynamical properties.

The variable heat capacitors defining the gas layers are adapted to satisfy the first law of thermodynamics:

$$\frac{dU_g^i}{dt} = \dot{m}_g^i \mathbf{h_g^i} - P_g^i \frac{dV_g^i}{dt} \tag{2}$$

where U_g and $\mathbf{h_g}$ are respectively the internal energy and the specific enthalpy of the hydrogen gas at pressure P_g and for a volume V_g. During the compression or the expansion stage strictly, the first term of right hand side in Eq. 2 depending on the mass flow rate $\dot{m}_g$ is null as the valves are closed. The superscript i stands for the i-th gas layer. Heat transfer by conduction with the adjacent layer is taken directly into account with the two thermal conductors, while conjugate heat transfer through the solid wall is taken into account through the thermal resistor. Thus equation 1 is layer dependent.

Heat transfer between the highest gas layer and the top wall surface is neglected due to the higher thickness of the tank there. At the interface between the lowest gas layer and the liquid volume, heat transfer $\dot{Q}_{gl}$ is defined as:

$$\dot{Q}_{gl} = S_p h_{gl}(T_l - T_g) \tag{3}$$

S_p is the piston area and h_{gl} is coefficient of gas-to-liquid heat transfer, also estimated with a Reynolds-Prandtl correlation.

The number of gas layers n is fixed to 20, which has shown to be sufficient to predict the temperature gradient and to achieve independence of the results on n. The layers are defined with identical hydrogen mass at all time, and their volumes can thus be different depending on the thermodynamical properties of the gas within the layer. To ensure that the pressure is identical in all layers, a stable dynamics procedure is implemented such as in (Srivatsa and P. Y. Li 2018), which depends on a small positive number λ and reads:

$$\frac{d(P_g^{i+1} - P_g^i)}{dt} = -\lambda(P_g^{i+1} - P_g^i) \tag{4}$$

Here, $\lambda = 1e^{-4}$ is sufficient to force the pressure to be equal in all gas layers. As for the liquid volume finally, a 0D zonal approach is used, for which the volume follows the first law of thermodynamics:

$$\frac{dU_l}{dt} = \dot{m}_l \mathbf{h_l} + \dot{Q}_{lg} \tag{5}$$

where $\dot{Q}_{lg} = -\dot{Q}_{gl}$ and $\mathbf{h_l}$ is the specific enthalpy of water. Due to the high thermal inertia of liquid water, its temperature increase remains much below 1^oC in all present simulations, however considering a fixed inlet temperature within the volumetric pump.

2.3 Material selection

Four materials were selected, representing both standard pressure vessels materials and materials with both high thermal effusivity and thermal diffusivity. Commercially available high-pressure vessels are all based on the use of aluminium, steels and carbon fiber reinforced plastics. The study focuses on structures based onto those three main types of materials. In the current study, both the thermal and mechanical properties of materials are considered, a priori, with the same level of importance regarding their impact on the compression energy consumption. Hence, best performing grades of steel and aluminium were chosen in terms of thermal effusivity and diffusivity and in terms of yield strength to density ratio (21.2.0 n.d.): AISI 316L, an austenitic stainless steels, and Al 7068, a 7000 aluminium series. To complete the selection, as metal hybrids and composites are also good material candidates for application as high-pressure vessels (Solazzi and Vaccari 2022) (Bhattacharyya, El-Emam, and Khalid 2022) (Liu et al. 2012), the following two materials are also investigated: a metal matrice composite (MMC), based on an aluminium matrix filled with carbon fibers, and a carbon fiber reinforced polymer (CFRP),

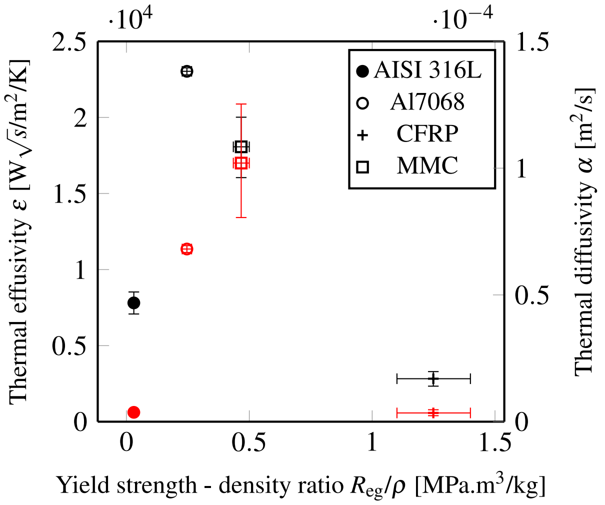

Figure 5. Variations of the selected materials thermal and mechanical properties. Thermal effusivities are represented in black while thermal diffusivities are represented in red.

based on an epoxy matrix reinforced by high strength unidirectional carbon fibers.

The mean thermal and mechanical properties of the four materials are presented **Table 1** and **Table 2**, respectively. **Figure 5** presents the variations of the thermal diffusivity and effusivity of those materials as a function of the ratio between the material yield strength and its density, thus relating the thermal and the mechanical properties of interest for this study.

For each material selected, the minimum wall thickness is determined by both the size of the reservoir and the targeted maximum gas pressure $P_{g,max}$. Thickness and diameter of the pressure vessels are the two main design criteria to ensure strength (Vullo et al. 2014). In the present study, the diameter of the vessel is fixed by the volume of gas that it must contain. Therefore, following recent ISO standard 9809-1:2019 for high pressure gas cylinder (*ISO 9809-1:2019: Gas cylinders - Design, construction and testing of refillable seamless steel gas cylinders and tubes - Part 1: Quenched and tempered steel cylinders and tubes with tensile strength less than 1 100 MPa* 2019), the cylinder wall thickness is obtained from the Lamé von Mises formula. It varies linearly with the vessel diameter D following:

$$a = \frac{D}{2}\left(1 - \sqrt{\frac{10FR_{eg} - \sqrt{3}P_{g,max}}{10FR_{eg}}}\right), \tag{6}$$

where R_{eg} is the minimum guaranteed value of yield stress and $F = min(\frac{0.65}{R_{eg}/R_{mg}}, 0.85)$ is a safety factor which depends on both R_{eg} and R_{mg}, the minimum guaranteed value of tensile stress. Assuming a perfect cylindrical shape for the piston, which is a general simplification of the real design of pressure vessel, the volume of material required is directly deduced, and so is the total mass required. Figure 6 shows this mass normalized by the max-

Table 1. Mean thermal properties of the selected materials.

Thermal property	Al 7068	CFRP	MMC	AISI 316L
Thermal conductivity $[W/m/K]$	190	5.25	182	15
Specific heat capacity $[J/kg/K]$	975	971	795	510
Density $[kg/m^3]$	2850	1565	2250	7970
Thermal diffusivity $[m^2/s^{-1}]$	6.81E-05	3.45E-06	1.02E-04	3.69E-06
Thermal effusivity $[J/m^2/s^{1/2}/K]$	23030	2820	18070	7810

Table 2. Mean mechanical properties of the selected materials.

Mechanical property	Al 7068	CFRP	MMC	AISI 316L
Yield strength [MPa]	702	1955	1050	240
Tensile strength [MPa]	740	1955	1050	522

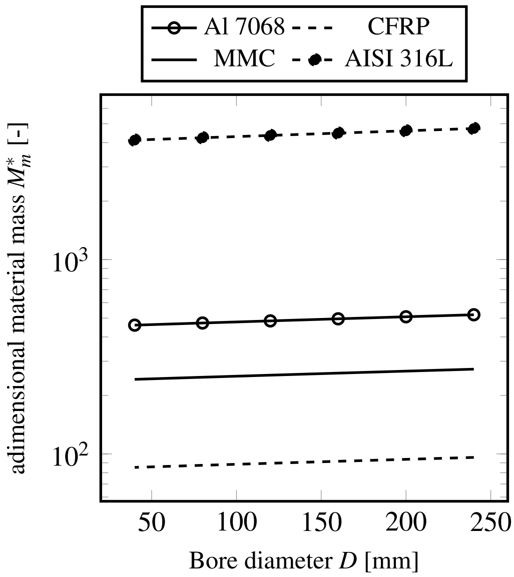

Figure 6. Variations of the selected materials mass required to sustained a 450 bar compression for diffrent cylinder diameter.

imum mass of gas (where the gas density ρ_g is taken at the initial baseline conditions). It highlights that the decrease of the piston thickness compensates the supplementary material needed for smaller piston. Hence, looking strictly only at the material mass required, the smaller the piston, the better it is.

3 Results

The conjugate thermal model described in the previous section has been used to predict the compression work required and heat production (through the effective temperature ratio) during the compression strokes. Salient results are presented in this section. First, time-resolved data are inspected in a baseline configuration. The influence of the stroke speed on the thermal gradient within the gas volume and compression work required are investigated. Second, the sentivity of the energy compression cost to the wall material is assessed.

The energy compression cost $\bar{C}$ is defined based on the energy requirement of the hydraulic pump. Further, it is defined per unit of mass of hydrogen discharged at the targeted pressure. The cost thus reads:

$$\bar{C} = \frac{\int Q_v |P_{g,left} - P_{g,right}|}{\int (q_{m,left} + q_{m,right})} \tag{7}$$

where q_m are the mass flow rates through the two exhaust check valves. The energy compression cost is assessed when the thermal transient behaviour of the system is over and a purely periodic state is reached. A final water level threshold of $99,5\%$ of the stroke length is considered, triggering the switch from the discharge stage to the expansion stage. This level corresponds directly to a dead volume of $0,5\%$ within both cylinder tanks. To sum up, Table 3 lists the geometrical, initial, and operating conditions of the present system in the baseline scenario.

Table 3. Geometrical, initial, and operating conditions of the liquid piston system.

Geometrical conditions	
Cylinder bore (internal)	240 mm
Cylinder stroke	1 m
Initial conditions	
Initial hydrogen pressure	15 bar
Initial hydrogen temperature	20 ^oC
Initial water level	0.4 m (L) & 0.6 m (R)
Initial water temperature	20 ^oC
Operating conditions	
Overall pressure ratio	30
Injection flowrate	0.8 L/s
Ext. ambiant temperature	20 ^oC
Ext. heat transfer coefficient	3 $W.K^{-1}.m^{-2}$

3.1 General results

Figure 7 presents the evolution of different thermophysical variables for fixed regime of pump operation, corresponding to a water flow rate of $Q_v = 0.8L/s$. Pressure rise is shown for both cylinders, as well as the temperature evolution of the left cylinder wall, and, bottom and top gas layers. Vertical delimiters separate the four stages of the compressor system: (i) a long compression stage higlighting the polytropic evolution of pressure and temperature, (ii) a short discharge stage where hydrogen is exhausted at constant pressure and fluctuating temperature, (iii) a short expansion stage where the remaining mass of hydrogen within the dead volume is expanded until the piston pressure reaches the inlet pressure, and finally (iv) a long admission stage where the hydrogen is filled again at constant inlet pressure, and which corresponds to the compression and discharge stage of the other piston. Pressure and temperature are normalized by their initial values (15bar, 20^oC). Aluminium is considered for the material wall, its maxium temperature reaching 35.6^oC at the end of the compression, i.e an extra 15^oC. As for the gas, the temperature ratio reaches 2.11 in the highest gas layers. This finally leads to a compression cost of $1.85kWh/kg$. Due to the heat conduction within the gas volume, the hydrogen temperature is not uniform as shown by the lower temperature obtained in the first layer ($R_T = 1.73$ at maximum).

Figure 8 shows how reducing the pump flow rate allows for more time to cool down the gas during compression, and reduces the vertical temperature gradient. In the second configuration, the flow rate has been divided by a factor height, and so is the power density which is proportional to the stroke duration. The temperature ratio reaches 1.88 at maximum at the end of the compression in this case. It corresponds to an energy cost of compression of $1.73kWh/kg$, representing a 8% cost reduction in comparison to the high flow rate scenario.

3.2 Sensitivity to the cylinder material

In this section, the energy cost of compression obtained with the present model is compared for the four different wall materials considered. The results are shown in Figure 9 along with the associated maximum temperature ratio at the end of the compression stage. Two scenarios are considered. For the first scenario, the internal gas-to-wall heat transfer is modeled with the Reynolds-Prandtl correlation calibrated for this specific liquid piston system in (Solai, Specklin, and Deligant 2025). Results (in light grey in Figure 9) highlight the negligible influence of the wall material in these conditions. The maximum relative difference for the compression cost is below 0.3%. Although the materials exhibit different thermal properties, the relatively short stroke time (around $56s$) and low gas-to-wall convective heat transfer coefficient (at maximum $340W/m^2/K$ at the end of compression and $100W/m^2/K$ in average) do not allow for the wall to affect the temperature rise within the cylinders.

In the second scenario, the heat transfer coefficient has been increased and fixed to $1500W/m^2/K$. This high value corresponds to what can be achieved when aiming at heat transfer enhancement through forced convection, as detailed in (Specklin et al. 2022) where the presence of a high speed fan in the cylinder is modeled. With the present model, this forced convective cooling reduces the energy cost of compression from $1.85kWh/kg$ to approximately $1.55kWh/kg$. Further, in this configuration, the influence of the wall material type becomes visible. Hence, a 2% difference is found in the energy cost of compression between the stainless steel and the carbon fiber reinforced polymer. Their thermal diffusivities and effusivities being relatively close, it shows that it is the thermal inertia which actually drives the energy cost among the material properties. The CFRP heat capacity is 16 folds smaller than the AISI 316L heat capacity, due to its high strength properties that allows for thinner wall and thus lower mass. Hence, after a thermodynamic periodic state being reached, the CFRP wall experiences temperature variations from 27^oC to 62^oC during a stroke, while the stainless steel wall only exhibits temperature periodic oscilations from 40^oC to 42^oC only.

To conclude, although it seems low, a 2% difference in the energy cost of compression can quickly add-up for expensive processes such as high pressure hydrogen compression. This result suggests then that there may be an interesting trade-off between the material cost for the compression system and the energy cost of the compression process.

4 Discussion

The results obtained with the present model can be put in perspective with those from the CFD investigations from (Specklin et al. 2022). In the latter, a lower energy cost of compression was obtained, $1.67kWh/kg$ at a power density of $540kW/m^3$, for an identical hydrogen compression configuration. There are however two differences in the modeling techniques that all lead to an overestimation of the cost in the present case or an underestimation in (Specklin et al. 2022). First, a Nusselt-Peclet correlation is used in (Specklin et al. 2022) for the unsteady gas-to-wall heat transfer, leading to higher coefficent values than the Reynolds-Prandtl correlation used in the present case. Second, Specklin et al. neglected the conjugate heat transfer and assumed an isothermal conditions for the internal wall which could slightly overestimates its cooling power. In our future studies, the Nusselt-Peclet correlation, together with a real gas media or Equation Of State, will be implemented in Modelica and will be used to bridge the modeling gap. Finally, a common limitation to both lumped model and CFD approaches is the omission of the liquid to vapor phase change during the process. The significance of this phenomena has yet not been clearly quantified in literature (Specklin et al. 2022) and certainly depends on gas nature and operating conditions. With air at low pressure ratio, the impact of evaporation seems to have a limited influence on the energy cost of compression (Solai, Specklin, and Deligant 2025). At high pressure ratio, it was shown theoretically by (Srivatsa and P. Y. Li 2018) that mass transfer between liquid water and vapor can significantly affect the maximum temperature reached during compression, and thus the energy cost. However, Wieberdink et al. (Wieberdink et al. 2018) did not mention this issue for instance during the operation of their liquid-piston system for air compression at similar ratio

DOI 10.3384/ecp2181001

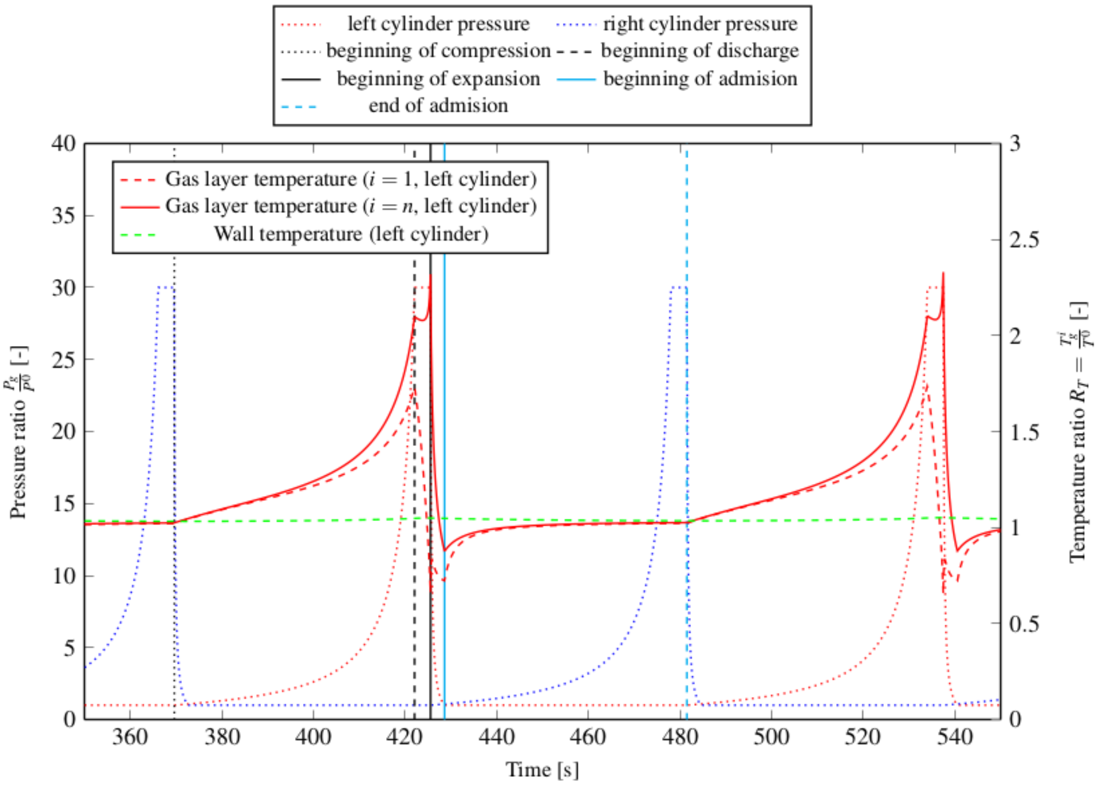

Figure 7. Evolution of pressures and temperatures obtained for $Q_v = 0.8L/s$ with aluminium wall.

and maxima of pressure. To avoid this issue, ionic liquid can be used to compress the gas, as they do not have a vapor pressure (Wang et al. 2018), or additional separator technologies to recover the purity of the materials but with additional costs.

5 Conclusion

In this paper, an object-oriented modeling methodology using the Modelica Programming Language has been presented for a high pressure liquid piston compressor system. The model is based on an existing experimental test bench using air, and has been extended for hydrogen gas. The modeling strategy involves considering the temperature gradient within the compressed gas, using a 1D discretization technique based on MSL elements. Further, conjugate heat transfer through the piston wall is considered and a specific attention is paid to the material choice. In its present state, the lumped model overestimates the energy cost of compression, in comparison to figures obtained with more accurate numerical investigations. However, the developed dynamic model is able to respond to changes in operating conditions and wall material types, and by means of this, it could be used for optimizing processes. In particular, promising insights can be expected from possible trade-off between material cost and energy cost, which could be investigated in full Life Cycle Analysis (LCA) or eLCC (environmental Life Cycle Costs) studies.

Acknowledgements

The authors declare that they have no known competing financial interests or personal relationships that could have appeared to influence the work reported in this paper.

References

21.2.0, Ansys Granta EduPack software (n.d.). "ANSYS, Inc., Cambridge, UK, 2021 (www.ansys.com/materials)". In: ().

Bhattacharyya, Rupsha, Rami S El-Emam, and Farrukh Khalid (2022). "Multi-criteria analysis for screening of reversible metal hydrides in hydrogen gas storage and high pressure delivery applications". In: *International Journal of Hydrogen Energy*.

ISO 9809-1:2019: Gas cylinders - Design, construction and testing of refillable seamless steel gas cylinders and tubes - Part 1: Quenched and tempered steel cylinders and tubes with tensile strength less than 1 100 MPa (2019-10). Standard. Geneva, CH: International Organization for Standardization.

Liu, P F et al. (2012). "Numerical simulation and optimal design for composite high-pressure hydrogen storage vessel: A review". In: *Renewable and Sustainable Energy Reviews* 16.4, pp. 1817–1827.

Maccarini, Alessandro et al. (2023). "Low-order aquifer thermal energy storage model for geothermal system simulation". In: *Proceedings of the 15th International Modelica Conference 2023, Aachen, October 9-11* 204.October, pp. 389–396. DOI: 10.3384/ecp204389.

Mazzucco, Andrea et al. (2016). "Integration of phase change materials in compressed hydrogen gas systems: Modelling and parametric analysis". In: *International Journal of Hydrogen Energy* 41.2, pp. 1060–1073. ISSN: 03603199. DOI:

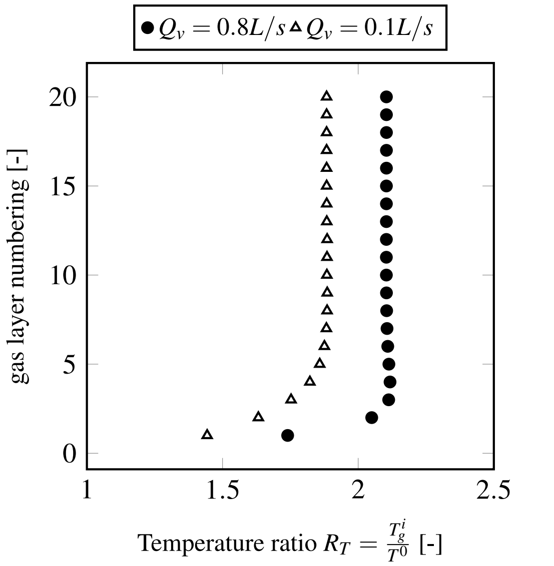

Figure 8. Non-dimensional temperature profiles along the vertical direction of the cylinder tank at the end of the compression stroke, for two different pump flow rates.

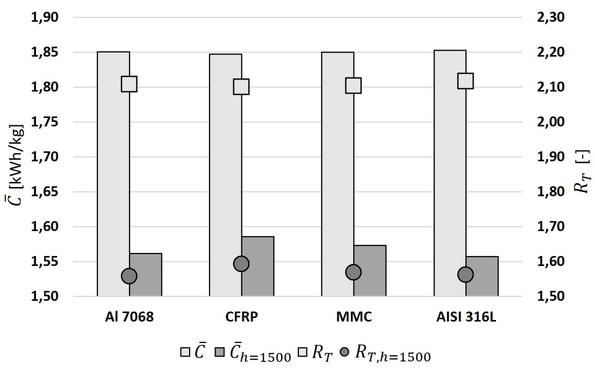

Figure 9. Specific energy cost for different wall materials with two internal convection cases

10.1016/j.ijhydene.2015.09.034. URL: http://dx.doi.org/10.1016/j.ijhydene.2015.09.034.

MSL (2023). Version 3.2.2. URL: https://github.com/modelica/ModelicaStandardLibrary.

OpenModelica (2023). Version 1.24.4. URL: https://openmodelica.org/ (visited on 2024-11-23).

Patil, Vikram C., Pinaki Acharya, and Paul I. Ro (2019). “Experimental investigation of heat transfer in liquid piston compressor”. In: *Applied Thermal Engineering* 146.June 2018, pp. 169–179. ISSN: 13594311. DOI: 10.1016/j.applthermaleng.2018.09.121. URL: https://doi.org/10.1016/j.applthermaleng.2018.09.121.

Saadat, M., P.Y. Li, and T.W. Simon (2012). “Optimal trajectories for a liquid piston compressor/expander in a Compressed Air Energy Storage system with consideration of heat transfer and friction”. In: *2012 American Control Conference (ACC)*, pp. 1800–1805. DOI: 10.1109/ACC.2012.6315616.

Sapin, Paul et al. (2018). “Dynamic modelling of water-droplet spray injection in reciprocating-piston compressors”. In: *ECOS 2018 - Proceedings of the 31st International Conference on Efficiency, Cost, Optimization, Simulation and Environmental Impact of Energy Systems* June.

Şeren, Erdoğan Mert and Mutlu İpek (2023). “Dynamic Modeling and Experimental Validation of Dishwasher with Heat Pump System”. In: *Proceedings of the 15th International Modelica Conference 2023, Aachen, October 9-11* 204, pp. 347–356. DOI: 10.3384/ecp204247.

Solai, Elie, Mathieu Specklin, and Michaël Deligant (2025). “Assessment of liquid piston compression efficiency through uncertainty analysis based on experimental measurements and 0D system modeling”. In: *Energy Conversion and Management* 326.December 2024, p. 119431. ISSN: 01968904. DOI: 10.1016/j.enconman.2024.119431. URL: https://doi.org/10.1016/j.enconman.2024.119431.

Solazzi, Luigi and Marco Vaccari (2022). “Reliability design of a pressure vessel made of composite materials”. In: *Composite Structures* 279, p. 114726.

Specklin, Mathieu et al. (2022). “Numerical study of a liquid-piston compressor system for hydrogen applications”. In: *Applied Thermal Engineering* 216.July, p. 118946. ISSN: 13594311. DOI: 10.1016/j.applthermaleng.2022.118946. URL: https://doi.org/10.1016/j.applthermaleng.2022.118946.

Srivatsa, Anirudh and Perry Y. Li (2018). “How moisture content affects the performance of a liquid piston air compressor/expander”. In: *Journal of Energy Storage* 18.August 2017, pp. 121–132. ISSN: 2352152X. DOI: 10.1016/j.est.2018.04.017. URL: https://doi.org/10.1016/j.est.2018.04.017.

Van de Ven, James D. and Perry Y. Li (2009). “Liquid piston gas compression”. In: *Applied Energy* 86.10, pp. 2183–2191. ISSN: 03062619. DOI: 10.1016/j.apenergy.2008.12.001. URL: http://dx.doi.org/10.1016/j.apenergy.2008.12.001.

Vullo, Vincenzo et al. (2014). “Circular cylinders and pressure vessels”. In: *Stress Analysis and Design; Springer: Berlin/Heidelberg, Germany*.

Wang, Ying et al. (2018). “Research on the design of hydrogen supply system of 70 MPa hydrogen storage cylinder for vehicles”. In: *International Journal of Hydrogen Energy* 43.41, pp. 19189–19195. ISSN: 03603199. DOI: 10.1016/j.ijhydene.2018.08.138. URL: https://doi.org/10.1016/j.ijhydene.2018.08.138.

Wieberdink, Jacob et al. (2018). “Effects of porous media insert on the efficiency and power density of a high pressure (210bar) liquid piston air compressor/expander – An experimental study”. In: *Applied Energy* 212.August 2017, pp. 1025–1037. ISSN: 03062619. DOI: 10.1016/j.apenergy.2017.12.093. URL: https://doi.org/10.1016/j.apenergy.2017.12.093.